JOURNAL OF MATERIALS SCIENCE 20 (1985) 53–59

# The influence of temperature and loading rate on flow and fracture of partially stabilized zirconia

JAMES LANKFORD
*Department of Materials Sciences, Southwest Research Institute, San Antonio, Texas 78284, USA*

The flow and fracture behaviour of magnesium stabilized partially stabilized zirconia subject to compressive loading is characterized for a wide range of strain rates and temperatures. It is found that the material exhibits plastic flow from 23 to 1200° C, and that the flow stress curve is serrated. Contrary to results for $Al_2O_3$, SiC and $Si_3N_4$, the strain rate dependence of compressive strength for partially stabilized zirconia (PSZ) does not correlate with the stress intensity dependence of subcritical crack growth velocity. These results, combined with the presence of an unusual type of deformation banding, are interpreted in terms of plastic strain-induced, co-operative martensitic transformation of metastable precipitates.

## 1. Introduction

Recently, the author reported [1] the results of a study of the compressive behaviour of partially stabilized zirconia (PSZ). The experiments, performed at room temperature and moderate loading rates, demonstrated that failure was preceded by significant plastic flow, behaviour which is uncharacteristic of tensile fracture. It was found that the plasticity resulted from unusual deformation bands, and suggested that the latter form by the co-operative, strain-induced martensitic transformation of metastable tetragonal precipitates.

However, many potential applications (bearings, engine components) of partially stabilized zirconia involve a compressive state of stress, rapid loading, and temperatures between 23 and ~1000° C. Furthermore, it already is known that elevated temperatures tend to degrade the outstanding tensile strength and fracture toughness which PSZ exhibits under ambient conditions. This paper therefore describes the results of an investigation which extends the previous compressive work into the projected operational regime.

## 2. Experimental procedures

The same magnesium stabilized ceramic* studied earlier [1] was used in the present experiments; materials and mechanical properties are characterized in Table I. Specimens were provided in the form of as-sintered right circular cylinders, with a length of 0.625 cm, and a diameter of 0.3125 cm. Special care was taken to precision grind and lap parallel to within 2 $\mu$m the ends of both the specimens and their alumina loading platens.

Compression tests were performed at strain rates ranging from $7 \times 10^{-5}$ to $1 \times 10^{3}$ $sec^{-1}$; low and intermediate rates were achieved using a standard servo-controlled test machine, while the fastest tests were accomplished by means of a Hopkinson pressure bar system. Since the load response of the material was found to be nonlinear, duplicate experiments were performed in load control, for low loading rates, with crosshead displacement monitored in order to characterize the approximate plastic strain prior to failure. Elevated temperature tests (to ~1200° C) were

*Nilsen TS-Grade PSZ; Nilsen Sintered Products, Ltd, Northcote, Victoria, Australia.

0022–2461/85 $03.00 + .12 

TABLE I Ambient material and mechanical properties*

| Tensile strength (4 bend) (MPa) | Vickers hardness (GPa) | Fracture toughness (MPa $m^{1/2}$) | Grain size ($\mu$m) |
|---|---|---|---|
| 600 | 10.2 | 8–15† | ~ 60 |

*Data from Nilsen Sintered Products, Ltd.
†Toughness variable due to $R$-curve behaviour.

run in a resistance-heated furnace within a dry argon environment.

In order to establish the threshold stress level for microfracture, acoustic emission (AE) was employed. The PZT transducer, resonant at 160 kHz, operated within the frequency range 100 kHz to 1 MHz. Since high temperatures were involved, the transducer was affixed to the loading ram; ambient environment experiments indicated that the signal amplitude due to microfracture events was not significantly reduced by positioning the transducer away from the specimen itself.

Optical and scanning electron microscopy were used to characterize damage mechanisms and post-failure fractography. In order to accomplish the former, extremely smooth (0.05 $\mu$m diamond finish) flats were polished onto certain specimens prior to testing. These were loaded to stress levels above yield, but below the ultimate strength, unloaded, and inspected microscopically. Specimens were coated with palladium in order to enhance optical contrast, and to permit SEM study.

Finally, the hardness of the PSZ was determined as a function of temperature to 800° C. Hardness tests were performed using a modified Tukon microhardness tester; the specimen and Vickers diamond pyramid indenter were immersed in argon and heated by a small resistance furnace. Indenter loads ranged from 200 to 800 g, over which range hardness was approximately independent of load.

## 3. Results

The effect of temperature ($T$) on compressive strength ($\sigma_c$) for strain rates ($\dot{\epsilon}$) of $7 \times 10^{-5}$, 0.2, and $10^3$ $sec^{-1}$, are shown in Fig. 1; also shown is the temperature dependence of the acoustic emission damage threshold ($\sigma_{AE}$) for $\dot{\epsilon} = 7 \times 10^{-5}$ $sec^{-1}$. At low and intermediate loading rates, strength is essentially independent of temperature for $T \lesssim 1000°$ C, above which the strength at $\dot{\epsilon} = 7 \times 10^{-5}$ $sec^{-1}$ begins to drop. Conversely, $\sigma_c$ increases monotonically with $T$ at $\dot{\epsilon} = 10^3$ $sec^{-1}$ over the temperature range studied, i.e. to 700° C. It is interesting to notice the extremely good repeatability of the strength measurements; duplicate tests yield $\sigma_c$ values which agree within ~ 1%. This probably is a consequence of the fact that the specimens yield prior to failure, behaving more like metals rather than classical brittle ceramics.

The acoustic emission results for the lowest strain rate roughly parallel the corresponding compressive strength. However, $\sigma_c$ and $\sigma_{AE}$ diverge for $T \lesssim 500°$ C, indicating that microfracture events precede gross failure. Convergence of $\sigma_c$ and $\sigma_{AE}$ above 500° C suggests either that pre-failure microfracture does not occur, or that such events are different in nature from those which take place at lower temperatures, and do not provide significant AE. As will be seen, microscopy indicates that the latter is in fact the case.

It is helpful also to plot the strength data in terms of $\dot{\epsilon}$, as shown in Fig. 2 for $T = 23°$ C; also

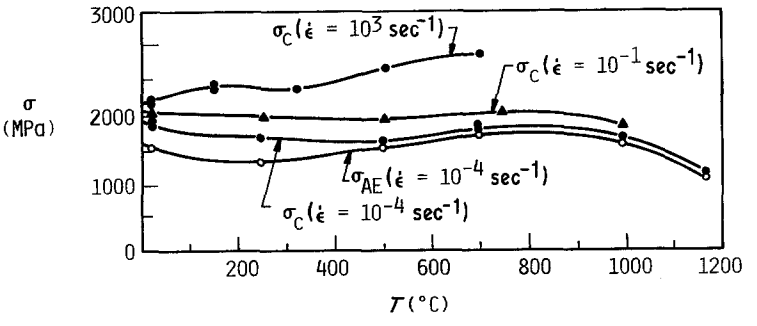


*Figure 1* Compressive strength ($\sigma_c$) and damage threshold stress level ($\sigma_{AE}$) against temperature.

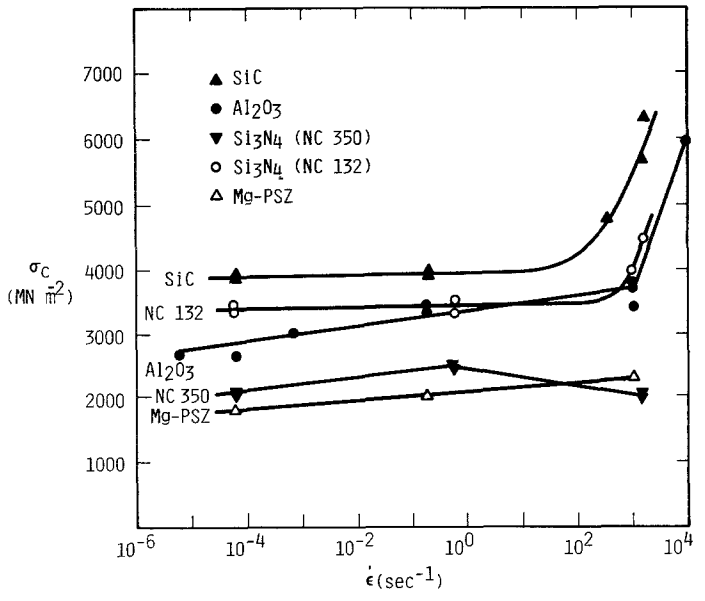


*Figure 2* Compressive strength against strain rate for various ceramics, $T = 23^\circ$ C.

shown are equivalent results* for other ceramics tested previously [2] by the author. Like these other materials, PSZ exhibits a linear log $\sigma_c$–log $\dot{\epsilon}$ dependence†, and as for $Al_2O_3$ and NC 350 ($\dot{\epsilon} \lesssim 10^1$ sec$^{-1}$), the slope of the PSZ relationship is low, but measurable. The significance of this parameter will be considered in the next section.

As mentioned earlier, PSZ tends to flow under the high stresses tolerated by compressive loading. Shown in Fig. 3 are the compressive strength and the yield strength ($\sigma_y$; defined as the apparent proportional limit) against temperature for $\dot{\epsilon} = 7 \times 10^{-5}$ sec$^{-1}$. Also plotted are the fracture toughness [3] ($K_{Ic}$), the hardness ($H_v$), and the three-point bend strength [4] ($\sigma_T$).

Although fracture toughness decreases quickly over the range $23^\circ$ C $< T < 500^\circ$ C, the other properties are much less sensitive to temperature until $T \gtrsim 1000^\circ$ C. Below $1000^\circ$ C, the plastic strain prior to failure averages 1.5%, over which range considerable strain hardening occurs, i.e. $\sigma_c/\sigma_y$ ranges from 1.27 to 1.5. As for $\sigma_c$, the tensile strength experiences a significant decrease once $T$ exceeds $1000^\circ$ C.

The plastic flow behaviour is complicated by transient load drops superimposed upon the strain hardening curve. This behaviour was demonstrated elsewhere [1] for ambient conditions; as shown in Fig. 4, it persists at elevated temperatures as well. The figure represents an actual experimental load–time trace for $T = 1000^\circ$ C, which shows that the serrations do not occur instantly after yielding, and that the failure strength is lower than the ultimate stress ($\sigma_{ULT}$) achieved in the test. At higher temperatures, the latter effect increases, until at $1168^\circ$ C, for example,

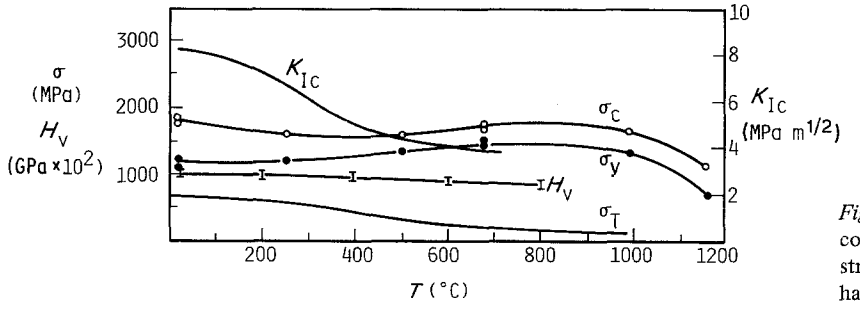


*Figure 3* Fracture toughness, compressive strength, yield strength, tensile strength and hardness against temperature.

*The behaviour for $\dot{\epsilon} \gtrsim 10^3$ sec$^{-1}$ is discussed elsewhere [2].
†Fig. 2 is plotted as $\sigma_c$ – log $\dot{\epsilon}$ in order to emphasize the slope.

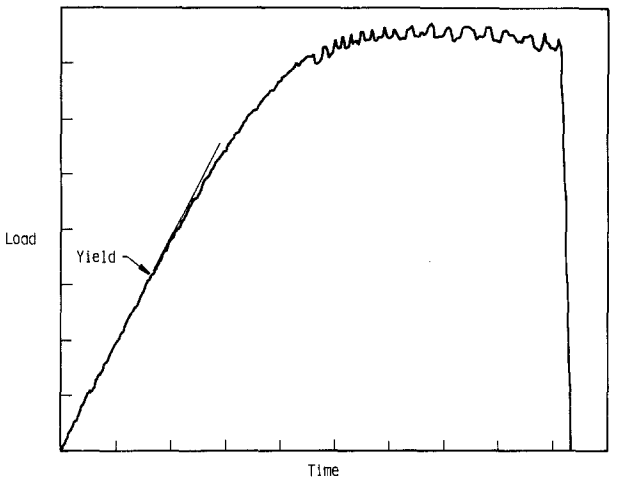


*Figure 4* Serrated load against time curve for $\dot{\epsilon} = 7 \times 10^{-5}$ sec$^{-1}$ and $T = 1000°$ C.

$\sigma_{ULT}/\sigma_c \simeq 1.2$. In addition, the serrations occur more frequently, and involve larger load drops, at higher temperatures.

Considerable insight regarding the basis of this behaviour can be derived from microscopy. As shown for $T = 23°$ C in Fig. 5, the strain-hardening, serrated flow stress region corresponds to the formation of axially-oriented transgranular microcracks, and what appears to be some sort of deformation bands. At higher temperatures, i.e. $T \gtrsim 600°$ C, the same situation prevails, with the exception that most of the axial microcracks now tend to lie along grain boundaries; the transition to intergranular microfracture is complete above $\sim 1000°$ C.

It is interesting to observe that the deformation bands, which are so strikingly visible in Nomarski optical illumination, are almost invisible in the scanning electron microscope (SEM). The edges of the bands, in particular, are nearly indiscernible, suggested that they do not consist of discrete ledges, and so differ from classical slip bands. The edges of the latter enhance secondary electron emission, and generally show up quite well in the SEM.

Optical examination and monitoring of acoustic emission indicates that the onset of axial microfracture correlates with the threshold stress for acoustic emission. Deformation bands begin to form in favourably oriented grains below this stress level, while the load drops in the stress–strain curve seem to correspond to prolific banding and associated surface rumpling [1] within the bulk of the specimen. In this regime, intersecting bands are formed due to the activity of multiple "flow" systems within individual grains.

## 4. Discussion

Transgranular microfracture apparently is responsible for pre-failure acoustic emission at $T \lesssim 500°$ C. Although intergranular microfracture likewise precedes failure at higher temperatures, this is a "quiet" process, which probably means that it takes place via grain boundary sliding, rather than rapid tensile rupture. This is borne out by the fact that SEM analysis of specimens unloaded just prior to failure at 1000° C showed that many surface grains already had extruded several micromillimetres out of originally smooth surfaces.

The author has shown elsewhere [2] that for $\dot{\epsilon} \lesssim 10^2$ sec$^{-1}$, $\sigma_c(\dot{\epsilon})$ tends to follow a relation-

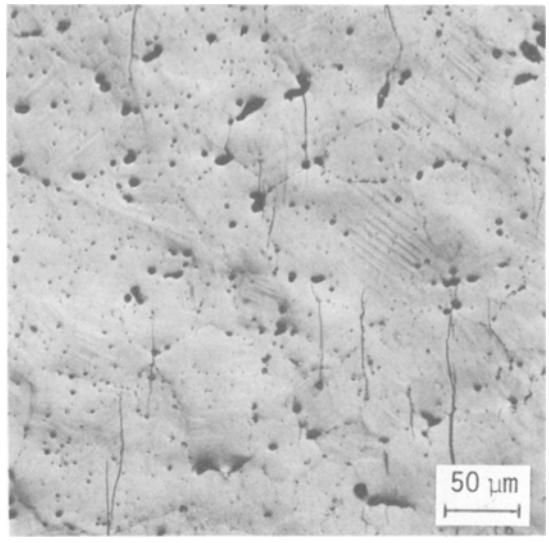


*Figure 5* Transformation bands and axial microfracture; $T = 23°$ C, $\sigma \simeq 90\%$, $\sigma_c$, $\epsilon \simeq 0.012$.

TABLE II Comparison of strength–strain rate and crack velocity–stress intensity exponents

| Material | $n_{(K-V)}$ | $n_T$ (Dynamic bending fatigue test) | $n_c$ (compression) |
|---|---|---|---|
| $Al_2O_3$ | 52 [5] | – | 51 |
| NC 350 | 57 [6] | – | 52 |
| NC 132 | very large [6] | – | very large |
| SiC | very large [7] | – | very large |
| Limestone | 130 [8] | – | 143 [11] |
| Mg–PSZ | 50–55 [9]* | 46–68 [10] | 95 |

*Li and Pabst [9] report an $n$ value of 80 for $K-V$ specimens with as-machined, residual-stressed surfaces; elimination of this machining damage by annealing yielded "true" $n$ values of 50 to 55.

ship of the form

$$\sigma_c \propto \dot{\epsilon}^{1/1+n_c} \quad (1)$$

where $n_c \approx n$ (Table II), the exponent in the crack growth relationship

$$V = AK^n \quad (2)$$

Here $V$ is the growth velocity of a Mode I tensile crack in a fracture mechanics-type specimen, $K$ is the stress intensity and $A$ is a material and environment-dependent constant. It already is well known that the failure of an unflawed brittle ceramic specimen tested in bending obeys a $\sigma_T(\dot{\epsilon})$ relationship of the form

$$\sigma_T \propto \dot{\epsilon}^{1/1+n_T} \quad (3)$$

in which the measured equivalence between $n_T$ and $n$ is accepted as proof that the strength–strain rate dependence is based upon thermally activated, tensile microcrack growth.

As shown in Table II, the behaviour of Mg–PSZ clearly violates the trend shown by the other materials listed. Although $n \approx n_T$, as expected, $n_c$ is nearly twice $n$, suggesting that something other than, or in addition to, subcritical crack growth, is responsible for the temperature dependence of $n$. Based on the observation of "deformation bands", and the serrated nature of the stress–strain curve, it seems likely that this other thermally activated mechanism is related to dislocations. Although this conclusion might seem rather inevitable, close consideration shows that the situation is rather more complex than it appears.

For example, it is thought that the enhanced fracture toughness of PSZ at ambient temperatures is caused by the free energy [12] of, or residual stress fields [13] associated with, the crack tip stress-assisted [14, 15] phase transformation of metastable precipitates from the tetragonal to the monoclinic structure. As the temperature rises, both the free energy associated with this martensitic transformation, and $K_c$, decrease, until at approximately 600° C, the net energy of transformation is negligible, and $K_c$ no longer decreases (Fig. 3). However, the transformation itself nevertheless persists to higher temperatures, and since there is always a shape change associated with the transformation, this might arguably account for the plasticity observed in the present experiments.

However, stress-induced martensitic transformations are strain rate independent. This suggests, as proposed earlier by the author [1] and, independently, Hannink and Swain [16], that the deformation bands produced under compressive loading are caused by a strain-induced [17, 18] martensitic reaction. In this case, the transformation is initiated by the microstress fields of dislocations nucleated within the cubic matrix and/or the tetragonal parent phase. The dislocations are envisaged to progress avalanche-fashion along zones of high shear stress, producing "deformation bands" of transformed material. Production of each band, or set of bands, would correspond to a load drop, and produce an increment of plastic strain.

The apparent structure of the transformation bands is sketched in Fig. 6. Hannink and Swain [19] have performed transmission electron microscopy on Mg–PSZ deformation bands identical in appearance to those reported, but produced in the compressive zones adjacent to indentations. Although the bands are composed of transformed monoclinic particles within a cubic matrix, the particles are characterized by two distinct internal microstructures. The first variant is coarse twinned, and found only inside the deformation bands; the second, fine-twinned type of monoclinic precipitate is located both within and without the bands.

An analogous situation is found in steels toughened by means of transformation-induced

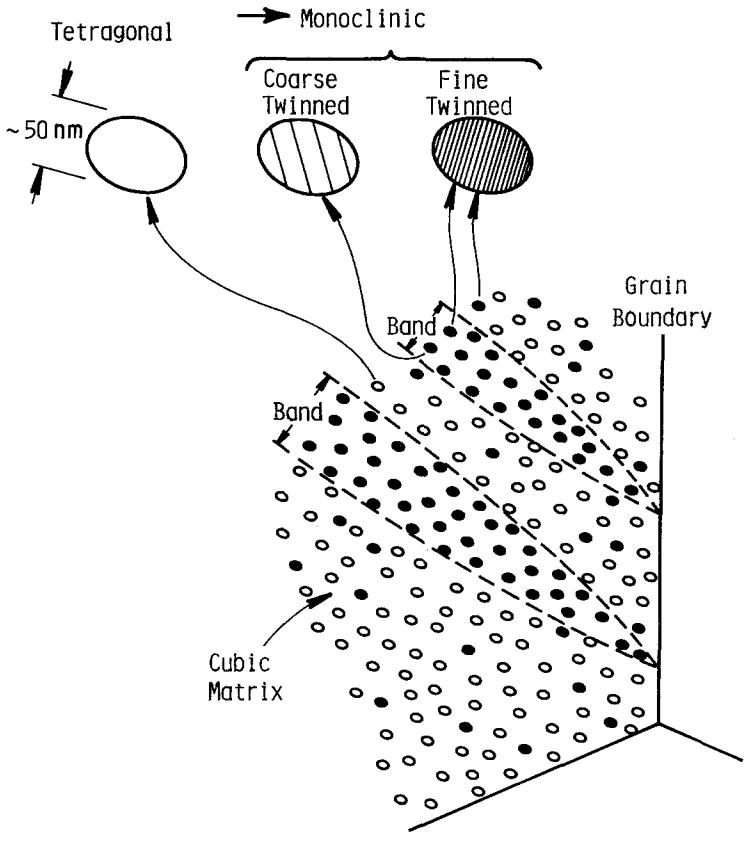


*Figure 6* Conceptual sketch of strain-induced co-operative transformation bands. Coarse-twinned monoclinic precipitates are strain-induced, and lie only within deformation bands. Fine-twinned particles formed during cooling below $M_s$, and possibly as a result of compressive stress-assisted transformation, and are therefore found throughout the microstructure.

plasticity (TRIP). Deformation of these steels produces serrated stress–strain curves, the smooth sections of which are interpreted [18, 20] in terms of (elastic) stress-assisted martensitic transformations, and the serrations in terms of (plastic) strain-induced transformations. It is generally found that the internal microstructure of stress-assisted martensite is identical to that which occurs spontaneously on cooling below $M_s$, but differs markedly from the characteristic of strain-induced martensite. Also, the strain-induced process becomes increasingly prevalent as the temperature of the deformation process rises [20].

In the case of Mg–PSZ, the presence of two transformation variants within the deformation bands clearly suggests that a strain-induced martensitic process is responsible for the bands. This is supported by the fact that the serrations become larger and more frequent with increasing temperatures, corresponding to increasingly easier dislocation activation. The fact that the band edges are so indistinct when viewed in the SEM can be understood in terms of their structure. As shown in Fig. 6, the bands are composed of an ensemble of transformed regions within an untransformed matrix; hence, there is no continuous boundary line analogous to a slip line.

To date, no TEM evidence for dislocation flow in PSZ has been observed [19, 21]. However, the search for dislocations in the complex and highly strained microstructure is very difficult [19], and the defects may be annihilated during the transformation process itself. Further research in this area is required.

## 5. Conclusions

It was found that the compressive behaviour of Mg–PSZ is unique relative to other strong ceramics. In particular, the material exhibits a serrated stress–plastic strain curve at all temperatures studied, and a strength–strain rate dependence which does not correlate with $K-V$ experiments. Co-operative transformation deformation bands form at all test temperatures. These results suggest that strain-induced martensitic transformations are important in high stress situations such as compression and indentation, while stress-assisted transformations probably are more relevant to crack tip (toughening) processes.

## Acknowledgements

The support of the Office of Naval Research under Contract No. N00014-75-C-0668 is gratefully acknowledged.

## References

1. J. LANKFORD, *J. Amer. Ceram. Soc.* 66 (1983) C-212.
2. *Idem*, "Fracture Mechanics of Ceramics", Vol. 5, edited by R. C. Bradt, A. G. Evans, D. P. H. Hasselman and F. F. Lange (Plenum Press, New York, 1983) p. 625.
3. M. V. SWAIN, private communication.
4. M. MARMACH, D. SERVENT, R. H. J. HANNINK, M. J. MURRAY and M. V. SWAIN, "Toughened PSZ Ceramics – Their Role as Advanced Engine Components", SAE Technical Paper 830318 (1983).
5. A. G. EVANS, M. LINZER and L. R. RUSSELL, *Mater. Sci. Eng.* 15 (1974) 253.
6. K. D. McHENRY, T. YONUSHONIS and R. E. TRESSLER, *J. Amer. Ceram. Soc.* 59 (1976) 262.
7. K. D. McHENRY and R. E. TRESSLER, *ibid.* 63 (1980) 152.
8. J. P. HENRY, J. PAQUET and J. P. TANCREZ, *Int. J. Rock Mech. Min. Sci. Geomech. Abstr.* 14 (1977) 85.
9. L. S. LI and R. F. PABST, *J. Mater. Sci.* 15 (1980) 2861.
10. J. D. HELFINSTINE and S. T. GULATI, *Ceram. Bull.* 59 (1980) 646.
11. S. J. GREEN and R. D. PERKINS, Proceedings of the Symposium on Rock Mechanics, edited by K. E. Gray (1968) p. 35.
12. F. F. LANGE, "Research of Microstructurally Developed Toughening Mechanisms in Ceramics", ONR Technical Report, Contract No. N00014-77-C-0441, June (1982).
13. R. M. McMEEKING and A. G. EVANS, *J. Amer. Ceram. Soc.* 65 (1982) 242.
14. A. G. EVANS and A. H. HEUER, *ibid.* 63 (1980) 241.
15. D. L. PORTER, A. G. EVANS and A. H. HEUER, *Acta Metall.* 27 (1979) 1649.
16. R. H. J. HANNINK and M. V. SWAIN, Proceedings of International Symposium on Plastic Deformation of Ceramics (Penn. State University, 1983) in press.
17. P. C. MAXWELL, A. GOLDBERG and J. C. SHYNE, *Metall. Trans.* 5 (1974) 1305.
18. D. FAHR, *ibid.* 2 (1971) 1883.
19. R. H. J. HANNINK and M. V. SWAIN, *J. Mater. Sci. Lett.* 16 (1981) 1428.
20. P. C. MAXWELL, A. GOLDBERG and J. C. SHYNE, *Metall. Trans.* 5 (1974) 1319.
21. A. H. HEUER, private communication.

*Received 20 January*
*and accepted 24 February 1984*